Spin-to-charge conversion in lateral and vertical topological-insulator/ferromagnet heterostructures with microwave-driven precessing magnetization

Farzad Mahfouzi,[1] Naoto Nagaosa,[2,3] and Branislav K. Nikolić[1,2,*]

[1]*Department of Physics and Astronomy, University of Delaware, Newark, Delaware 19716-2570, USA*

[2]*RIKEN Center for Emergent Matter Science (CEMS), Wako, Saitama 351-0198, Japan*

[3]*Department of Applied Physics, University of Tokyo, Tokyo 113-8656, Japan*

(Received 23 July 2014; revised manuscript received 17 August 2014; published 26 September 2014)

Using the charge-conserving Floquet-Green function approach to open quantum systems driven by an external time-periodic potential, we analyze how spin current pumped by the precessing magnetization of a ferromagnetic (F) layer is injected *laterally* into the interface with strong spin-orbit coupling (SOC) and converted into charge current flowing in the same direction. In the case of a metallic interface with the Rashba SOC used in recent experiments [J. C. R. Sánchez, L. Vila, G. Desfonds, S. Gambarelli, J. P. Attané, J. M. De Teresa, C. Magén, and A. Fert, Nat. Commun. **4**, 2944 (2013)], both spin I^{S_α} and charge I current flow within the interface where $I/I^{S_\alpha} \simeq 2$–8% (depending on the precession cone angle), while for a F/topological-insulator (F/TI) interface employed in related experiments [Y. Shiomi, K. Nomura, Y. Kajiwara, K. Eto, M. Novak, K. Segawa, Y. Ando, and E. Saitoh, arXiv:1312.7091] the conversion efficiency is greatly enhanced ($I/I^{S_\alpha} \simeq 40$–60%) due to perfect spin-momentum locking on the surface of a TI. The spin-to-charge conversion occurs also when spin current is pumped *vertically* through the F/TI interface with smaller efficiency ($I/I^{S_\alpha} \sim 0.001\%$), but with the charge current signal being sensitive to whether the Dirac fermions at the interface are massive or massless.

DOI: 10.1103/PhysRevB.90.115432 PACS number(s): 72.25.Mk, 73.40.−c, 85.75.−d

One of the central goals of second generation spintronics [1] is to generate and manipulate pure spin currents with no net charge flux. The pure spin currents make possible transport of information encoded in electron spin with much less dissipation than generated when using spin-polarized charge currents of first generation spintronics. However, their detection and measurement requires one to convert them into conventional charge currents and voltages. Over the past decade, the inverse spin Hall effect [2] (SHE)—where pure spin current injected longitudinally into a material with spin-orbit coupling (SOC) induces [3,4] transverse charge current—has emerged as a detector routinely coupled to generators of pure spin currents like spin pumping by precessing magnetization [5–7], nonlocal spin diffusion [8,9], direct SHE [10,11], magnon-spin transmutation [12], and laser pulses [13].

The very recent experiments [14,15] on lateral heterostructures illustrated in Fig. 1(a) have observed charge current I along the x direction in the absence of any applied dc bias voltage. In one heterostructure of this type [14], a ferromagnetic (F) layer with precessing magnetization driven by microwaves of frequency ω under the ferromagnetic resonance (FMR) condition is brought into a contact with an interfacial (as formed at a Ag/Bi interface [14]) two-dimensional electron gas (2DEG) with conventional parabolic energy-momentum dispersion and spin splitting described by the Rashba Hamiltonian [16]

$$\hat{H}_{\rm 2DEG} = \frac{\hat{\mathbf{p}}^2}{2m^*} + \frac{\alpha_{\rm R}}{\hbar}(\hat{\boldsymbol{\sigma}} \times \hat{\mathbf{p}}) \cdot \mathbf{e}_z. \tag{1}$$

In the other one [15], an F layer is brought into a direct contact with a 2D gas of massless Dirac electrons with linear energy-momentum dispersion residing on the surface of three-dimensional topological insulators (3D TIs), as described by the Hamiltonian [17]

$$\hat{H}_{\rm TI} = v_F(\hat{\boldsymbol{\sigma}} \times \hat{\mathbf{p}}) \cdot \mathbf{e}_z. \tag{2}$$

Here m^* is the effective mass ($m^*/m_e \simeq 0.35$ at the Ag/Bi interface) and v_F is the Fermi velocity. The key ingredient for the observed effect is that Hamiltonians in Eqs. (1) and

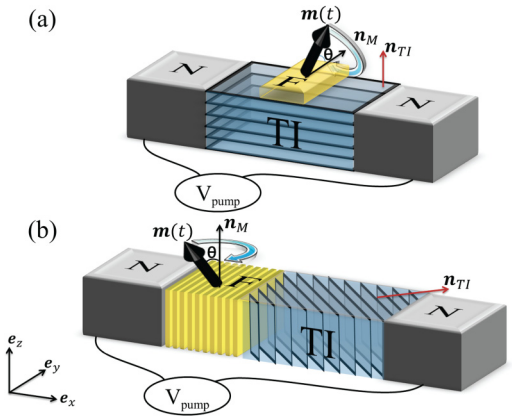

FIG. 1. (Color online) Schematic of (a) lateral and (b) vertical F/TI heterostructures whose precessing magnetization, driven by the absorption of microwaves of frequency ω under the FMR conditions, pumps pure spin current along the z or x axis, respectively, in the absence of any dc bias voltage between the semi-infinite N leads. The strong interfacial SOC converts pumped spins into charge current flowing along the x axis in both setups, which is measured as the voltage signal $V_{\rm pump}$ in an open circuit. Besides lateral heterostructures of an F/TI type in panel (a), we also study lateral F/2DEG heterostructures with conventional Rashba SOC at the interface for comparison. The unit vector $\mathbf{n}_M$ specifies the axis around which magnetization $\mathbf{m}(t)$ is precessing, while the vector $\mathbf{n}_{\rm TI}$ is perpendicular to quintuple layers (QLs) comprising the 3D TI slab [e.g., panel (b) illustrates the case $\mathbf{n}_{\rm TI} = (1,1,0)$].

*bnikolic@udel.edu

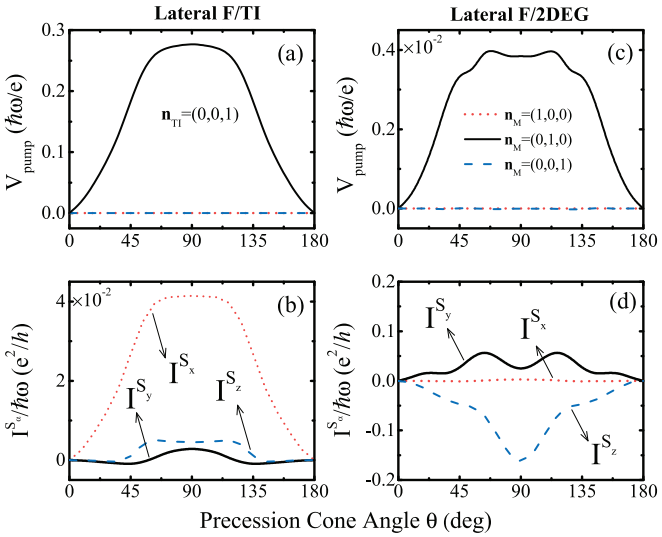

FIG. 2. (Color online) (a), (c) The angular dependence of the dc pumping voltage in lateral F/TI and F/2DEG heterostructures illustrated in Fig. 1(a) for different orientations of the axis $\mathbf{n}_M$ around which magnetization is precessing with a cone angle θ. Panels (b) and (d) show the spin current I^{S_α} which accompanies the charge current $I = V_{\text{pump}}G$ in (a) and (c), respectively, where both I^{S_α} and I flow along the x axis in Fig. 1(a). Note that charge current in panels (a) and (c) is nonzero only when magnetization is precessing around the y axis in Fig. 1(a).

(2) exhibit spin-momentum locking due to an interfacial SOC term in which $\hat{\mathbf{p}} = (\hat{p}_x, \hat{p}_y)$ is the momentum operator and $\hat{\boldsymbol{\sigma}} = (\hat{\sigma}_x, \hat{\sigma}_y, \hat{\sigma}_z)$ is the vector of the Pauli matrices. While these two Hamiltonians are quite similar, the main difference is that the SOC term in Eq. (1) is a perturbation on the top of the band kinetic energy, while in Eq. (2) it is the only term present. Another mechanism of pumped-spin-to-charge conversion using interfacial SOC was predicted theoretically in Ref. [18] for *vertical* F/I heterostructures, such as those illustrated in Fig. 1(b) using an F/TI combination, where pumped spins are reflected and transmitted *perpendicularly* through the interface with strong SOC which generates charge current along the x axis in Fig. 1(b).

Here we provide a unified treatment for both of these pumped-spin-to-charge conversion processes using a Floquet-nonequilibrium Green function (Floquet-NEGF) formalism [18,19] applied to a time-dependent Hamiltonian of lateral and vertical heterostructures depicted in Figs. 1(a) and 1(b), respectively. For simplicity, we assume a ballistic transport regime for both of them. For lateral heterostructures in Fig. 1(a), we demonstrate in Fig. 2 that *both* charge I and spin I^{S_α} currents will flow within the plane of an F/TI or F/2DEG interface in the x direction. The charge current in Figs. 2(a) and 2(c) is nonzero *only* when magnetization is precessing around the y axis—this setup injects a dc component of spin current into the interface with spins pointing along the y axis, which is partially converted into charge current along the x axis. On the other hand, when the F layer magnetization is precessing around the x or the z axis, the charge current along the x axis is identically zero ($I \equiv 0$), while nonzero pure spin currents I^{S_x} and I^{S_z}, respectively, continue to flow along the x axis, as shown in Figs. 2(b) and 2(d).

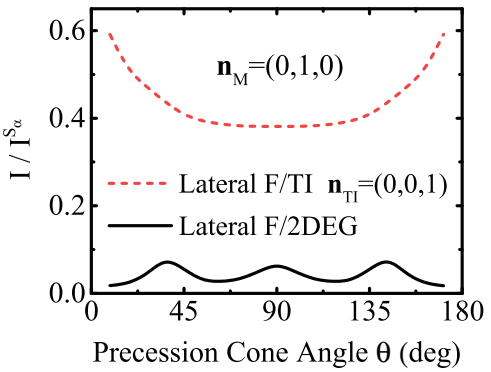

FIG. 3. (Color online) Efficiency of spin-to-charge conversion in lateral F/TI and F/2DEG heterostructures is quantified by the ratio of charge I to spin I^{S_α} currents from Fig. 2 for magnetization precessing around the y axis [$\mathbf{n}_M = (0,1,0)$] in Fig. 1(a).

The spin-to-charge conversion in lateral heterostructures in Fig. 1(a) has previously been interpreted as the "inverse Edelstein effect" [20] (IEE) where *nonequilibrium* spin density in the diffusive 2DEG spin split by SOC creates an electric field perpendicular to the spin direction. Such an electric field then drives charge current I, or induces the dc voltage signal $V_{\text{pump}}(\theta) = I(\theta)/G(\theta)$ in an open circuit where $G(\theta)$ is the conductance of a two-terminal system with static magnetization. In the case of heterostructures in Fig. 1(a), the required nonequilibrium spin accumulation arises due to spin current I^{S_α} pumped along the z axis by the precessing F layer, which is *diverted* to flow within the interface because of highly resistive Bi or TI layers. Such spin current along the x axis has a dc component carrying spins pointing in the y direction, so that charge current observed also along the x axis is *unrelated* to the inverse SHE. It has been speculated [15] that the efficiency of conversion in the case of F/TI heterostructures could reach its maximum ($I/I^{S_\alpha} \to \infty$) due to spin-momentum locking along the single circle [17] (formed in k space at the intersection of the Dirac cone energy-momentum dispersion and the Fermi energy plane), in contrast to spin-momentum locking along two circles [14,16,20] in the case of conventional massive electrons described by the Rashba Hamiltonian in Eq. (1) which counter the effect of each other.

However, the IEE-based explanations operate [15,20] with nonequilibrium spin density, rather than with time-dependent pumped spin current which is giving rise to it, so it has remained unclear how much of it is actually converted into charge current and how efficient are different types of SOC in this conversion process [21,22]. While our interpretation is qualitatively compatible with the one based on the IEE [20], our approach finding both charge and spin currents makes it possible to quantify the spin-to-charge conversion efficiency which we define as the ratio I/I^{S_α}. To quantify the total spin angular momentum emitted by the central region of systems in Fig. 1 into two normal metal (N) leads, we sum up the magnitudes of spin currents in the left (L) and the right (R) leads to get $I^{S_\alpha} = |I_L^{S_\alpha}| + |I_R^{S_\alpha}|$. Note that we employ the same units for charge current, $I = I^{\uparrow} + I^{\downarrow}$, and spin current, $I^{S_\alpha} = I^{\uparrow} - I^{\downarrow}$, expressed in terms of spin-resolved charge currents $I^{\uparrow}$ and $I^{\downarrow}$ carrying spins pointing along the α axis. Thus, the ratio I/I^{S_α} is a pure number which is plotted in Fig. 3

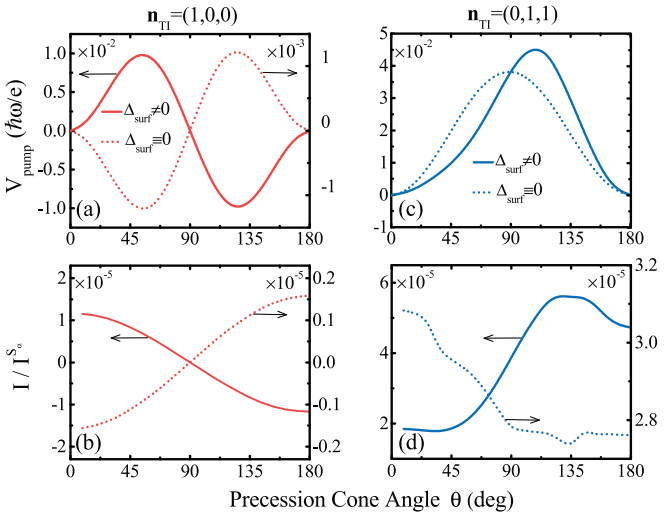

FIG. 4. (Color online) (a), (c) The angular dependence of the dc pumping voltage in F/TI vertical heterostructures illustrated in Fig. 1(b) whose magnetization is precessing around the z axis, $\mathbf{n}_M = (0,0,1)$. Panels (b) and (d) show the spin current I^{S_α} which accompanies the charge current $I = V_{\rm pump}G$ in (a) and (c), respectively, where both I^{S_α} and I flow along the x axis in Fig. 1(b). The QLs of the 3D TI slab are oriented perpendicular to $\mathbf{n}_{\rm TI} = (1,0,0)$ in panels (a) and (b), or perpendicular to $\mathbf{n}_{\rm TI} = (0,1,1)$ in panels (c) and (d).

for lateral heterostructures in Fig. 1(a). It reaches $I/I^{S_\alpha} \simeq$ 2–8% for the F/2DEG interface, and increases to $I/I^{S_\alpha} \simeq$ 40–60% for the F/TI interface. We note that in the case of conventional spin-polarized charge current, $0 < I^{S_\alpha}/I \leqslant 1$ is the component of the spin-polarization vector along the α axis. In Fig. 3 this number can be bigger than one because spin current was initially generated by pumping in the absence of any dc bias voltage and without any net charge flux, and subsequently only partially converted into charge current by the SO-coupled interface.

It is worth mentioning that the cone angle dependency of the voltage signal in Fig. 2(a) suggests that higher order perturbation terms have significant contribution to the results. This effect is even more pronounced at small cone angles where we find a linear dependency, in contrast the parabolic dependency in conventional F/N multilayers [23].

Figures 4(a) and 4(c) show charge current along the x axis in vertical heterostructures depicted in Fig. 1(b) whose magnetization is precessing along the z axis. In conventional F/N multilayers, magnetization dynamics pumps time-dependent pure spin current into the N layer which has been amply explored [23] as a robust and ubiquitous example of adiabatic pumping effect at room temperature. However, no charge pumping at the adiabatic level, i.e., with contribution proportional to ω, is expected in multilayers with a *single* precessing F layer [24]. In fact, in the absence of interfacial SOC F/I junctions can pump [24] charge current $\propto\omega^2$ which is, therefore, nonadiabatic and has a much smaller effect. This outcome changes if strong SOC is present directly at the interface, as predicted to occur in vertical F/I junctions with the Rashba SOC at the interface [18]. While the angular dependence of pumped charge current for the F/TI interface in Fig. 4(a) is the same $\propto \sin^2\theta\cos\theta$ as for the F/I interface with the Rashba SOC, the magnitude of the voltage signal is very sensitive to opening of the time-dependent energy gap $\Delta_{\rm surf}(t)$ on the surface of the TI by the magnetic proximity effect. That is, as soon as the cone angle θ becomes nonzero due to microwave absorption, the time-dependent exchange field acquires a component $(\Delta\sin\theta\sin\omega t)\mathbf{e}_x$ which is perpendicular to the surface of the TI and induces the corresponding surface gap $\Delta_{\rm surf}(t)$. The value of $\Delta^{\rm max}_{\rm surf}$ is not necessarily related to $\Delta|\sin\theta|$ because the magnetic proximity effect is influenced by the microscopic details [25] at the F/TI interface, so that in Fig. 4 we consider both $\Delta_{\rm surf}(t) \neq 0$ and $\Delta_{\rm surf}(t) \equiv 0$ cases.

The recent theoretical [25] and experimental [26] efforts have vigorously pursued F/TI heterostructures with nonzero (time-independent) $\Delta_{\rm surf}$, as well as without complicated hybridization [25] of bulk and surface states so that a split Dirac cone remains easily identifiable. Such a time-reversal-breaking-induced gapped surface state of 3D TI hosts massive Dirac fermions which make possible experimental probing of generic properties of 3D TIs like the topological magnetoelectric effect (where magnetization is generated by an electric field with a quantized coefficient), the half-integer quantum Hall effect, and the magnetic monopole [17]. It has also been predicted [27] that the F/TI heterostructure in Fig. 1(a) with precession axis lying within the TI surface will pump charge current which jumps abruptly at times when the z component of the precession magnetization touches zero, which is closely related to the parity anomaly in high energy physics. However, observation of such effects requires perfectly insulating bulk of TI and Fermi energy tuned close to the Dirac point (DP). On the other hand, the sensitivity of the charge current in Fig. 4(a) on the presence of $\Delta_{\rm surf}(t) \neq 0$ does not require either of these two conditions.

The Bi_2Se_3 realization of a TI is a strongly anisotropic material composed of QLs of Bi and Se atoms, where one QL consists of three Se layers strongly bonded to two Bi layers in between [17]. The electrons on the metallic surface of Bi_2Se_3 are often described by the effective Hamiltonian in Eq. (2) which accounts for spin-orthogonal-to-momentum locking for both Bi and Si sublattices observed in spin–angle-resolved photoemission spectroscopy (spin-ARPES) experiments [17]. However, such a description is valid only when the surface of the TI crystal coincides with the plane of the QL, while for other orientations of QLs the two sublattices generate different spin textures [28,29]. To illustrate their effect, Fig. 4(c) plots charge current when QLs are oriented perpendicularly to the vector $\mathbf{n}_{\rm TI} = (0,1,1)$ drawn in Fig. 1. The corresponding ratios I/I^{S_α} are plotted in Figs. 4(b) and 4(d) for two different orientations of QLs (denoted on the top of the left and the right columns in Fig. 4).

The nonzero pumping voltage $V_{\rm pump} \propto \omega$ in vertical F/I junctions with interfacial SOC is closely related [18] to the tunneling anisotropic magnetoresistance (TAMR). The out-of-plane TAMR for F/TI vertical heterostructures is defined [18] as $\text{TAMR}(\theta) = [R(\theta) - R(0^\circ)]/R(0^\circ)$ using conventional dc resistances $R(\theta)$ measured by tilting the static magnetization of the F layer in Fig. 1(b) away from the z axis. The TAMR curves in Fig. 5 show that change in the conductance $G(\theta) = 1/R(\theta)$

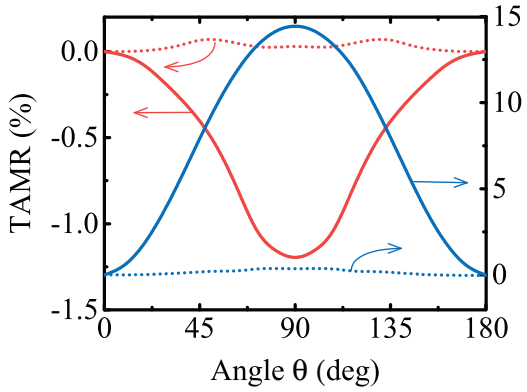

FIG. 5. (Color online) The TAMR of F/TI vertical heterostructures illustrated in Fig. 1(b) for a gapless ($\Delta_{\rm surf} \equiv 0$ for dotted lines) or gapped ($\Delta_{\rm surf} \neq 0$ for solid lines) surface of the TI that is in direct contact with the F layer. The QLs of the 3D TI slab are oriented perpendicular to $\mathbf{n}_{\rm TI} = (1,0,0)$ for curves with the left ordinate, or perpendicular to $\mathbf{n}_{\rm TI} = (0,1,1)$ for curves with the right ordinate.

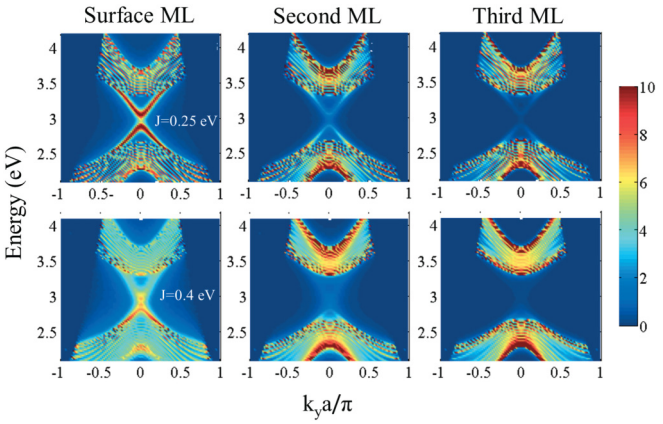

FIG. 6. (Color online) The local DOS $g(E,k_y,k_z = 0)$ on the surface ML of the TI slab in contact with the F layer within the vertical heterostructure illustrated in Fig. 1(b), as well as on the adjacent second and third MLs. In the top row of panels, the TI slab is weakly (F/TI hopping is $J = 0.25$ eV) coupled to the F layer, and in the bottom row of panels the coupling (F/TI hopping is $J = 0.4$ eV) is stronger. The static magnetization of the F layer is perpendicular to the F/TI interface, and it is assumed to induce an energy gap on the surface ML of TI via the magnetic proximity effect. The QLs of the TI slab are oriented perpendicular to $\mathbf{n}_{\rm TI} = (1,0,0)$.

is too small to account for the enormous difference between $V_{\rm pump}(\Delta_{\rm surf} \neq 0)$ and $V_{\rm pump}(\Delta_{\rm surf} \equiv 0)$ cases in Fig. 4(a). Although TAMR in Fig. 5 also differentiates between the presence or absence of massive Dirac fermions on the surface of the TI, it cannot be used reliably for this purpose since it would diminish when bulk charge carriers are present within the TI slab.

We now explain details of our approach to calculate pumped spin and charge currents. The F/TI and F/2DEG lateral heterostructures illustrated in Fig. 1(a) are modeled on a simple cubic or square tight-binding lattice with lattice spacing a, respectively. The TI central region has finite length $L_x^{\rm TI} = 50a$ and thickness $L_z^{\rm TI} = 8a$, while it is assumed to be infinite in the y direction, with each site hosting four spin-dependent orbitals of the minimal effective Hamiltonian [30]. The 2DEG central region has finite length $L_x^{\rm 2DEG} = 100a$, while it is assumed to be infinite in the y direction, with each site hosting two spin-dependent orbitals of the discretized version [31] of Hamiltonian in Eq. (1). We do not model explicitly the presence of the F overlayer with precessing magnetization in Fig. 1(a), but instead add term $-\Delta\mathbf{m}(t)\cdot\hat{\boldsymbol{\sigma}}/2$ in the region of length $L_x^{\rm F}$ residing in the center of the top plane of the TI or plane of 2DEG. Here Δ is the mean-field exchange splitting induced by the F overlayer through magnetic proximity effect and $\mathbf{m}(t)$ is the unit vector along the direction of precessing magnetization. For the case of a F/TI heterostructure, we select $L_x^{\rm F} = 20a$ and $\Delta = 0.28$ eV, while in the case of F/2DEG heterostructures we select $L_x^{\rm F} = 50a$, $\Delta = 0.2$ eV, and $\alpha_{\rm R}/2a = 0.1$ eV.

The vertical F/TI heterostructures in Fig. 1(b) are modeled on the simple cubic lattice composed of 2D monolayers (MLs) that are infinite in the yz plane. The thickness of the F layer is $L_x^{\rm F} = 50$ MLs and of the TI layer it is $L_x^{\rm TI} = 5$ MLs. In the case of vertical heterostructures, we add $-\Delta_{\rm surf}\mathbf{m}(t)\cdot\hat{\boldsymbol{\sigma}}/2$ on the first monolayer of the TI layer in contact with the F layer, where both $\Delta_{\rm surf} \equiv 0$ and $\Delta_{\rm surf} = \Delta$ ($\Delta = 0.28$ eV is the exchange splitting chosen in the bulk of the F layer) are considered in Figs. 4 and 5.

Figure 6 shows the local density of states (LDOS) on the MLs of a TI that are the closest to the F layer within the vertical heterostructure in Fig. 1(b). When the hopping parameter between the lattice sites of F and TI layers is large ($J = 0.4$ eV), the energy-momentum dispersion displayed in the bottom row of Fig. 6 bears little resemblance to the Dirac cone because of the flooding [32] of the F/TI interface by evanescent wave functions which originate from the F layer and penetrate into the bulk gap of TI layer while exponentially decaying along the x axis. To evade this effect, we assume smaller hopping $J = 0.25$ eV which leads to LDOS shown in the top row of panels in Fig. 6. In addition, Fig. 6 demonstrates how a gapped surface state of TI can penetrate into the bulk of TI as evanescent wave function decaying over the first few MLs, which effectively dopes the bulk.

The explicit expressions for the Hamiltonians discussed above, including how to properly couple the Hamiltonian of semi-infinite N leads or F layer with two orbitals per site to the TI Hamiltonian with four orbitals per site, can be found in Ref. [29] for the TI central region or in Ref. [31] for the 2DEG central region. The bottom of the band of the TI is shifted by 3.0 eV, so that the DP is at 3.0 eV and the Fermi energy is chosen at $E_F = 3.1$ eV for both lateral and vertical F/TI heterostructures in Fig. 1. The Fermi energy for lateral F/2DEG heterostructures is set at $E_F = 3.5$ eV in order to ensure that tight-binding dispersion reduces to a parabolic one.

Since pumped charge current and all components of the pumped spin current tensor are time-dependent in the presence of SOC [18,22], the NEGF formalism [33] is an advantageous choice for their computation because it gives from the outset experimentally measurable current averaged over one period. An alternative scattering matrix approach to adiabatic pumping [23,34] requires one to compute current at all times (or, in practice, over a discrete time grid) during one period

of microwave oscillations and then find its average [22,35], which can be very expensive computationally [especially for tunneling structures, like vertical F/TI ones in Fig. 1(b), where current amplitude is several orders of magnitude larger than its average value].

We compute pumped spin and charge currents in heterostructures in Fig. 1 using the recently derived [18] *exact* multiphoton solution to double-Fourier-transformed NEGFs in the presence of external time-periodic potential, which is adapted below to systems that are infinite in one or two directions. In terms of the operators $\hat{c}^{\dagger}_{n\sigma}$ ($\hat{c}_{n\sigma}$) which create (annihilate) an electron with spin σ on lattice site n, the two fundamental objects [33] of the NEGF formalism are the retarded $G^{r,\sigma\sigma'}_{nn'}(t,t') = -i\Theta(t-t')\langle\{\hat{c}_{n\sigma}(t),\hat{c}^{\dagger}_{n'\sigma'}(t')\}\rangle$ and the lesser $G^{<,\sigma\sigma'}_{nn'}(t,t') = i\langle\hat{c}^{\dagger}_{n'\sigma'}(t')\hat{c}_{n\sigma}(t)\rangle$ GF which depend on two time arguments. The former describes the density of available quantum states, while the latter describes how electrons occupy those states. Here $\langle\ldots\rangle$ denotes the nonequilibrium statistical average [33]. To solve the equation of motion for $\hat{G}^{r,\sigma\sigma'}_{nn'}(t,t')$ and the Keldysh integral equation for $G^{<,\sigma\sigma'}_{nn'}(t,t')$, it is advantageous to switch to a more convenient representation ($\hbar = 1$)

$$\mathbf{G}^{r(<)}(t,t') = \int_{-\infty}^{+\infty}\frac{dE}{2\pi}\int_{-\infty}^{+\infty}\frac{E'}{2\pi}\,e^{-iEt+iE't'}\mathbf{G}^{r(<)}(E,E'). \tag{3}$$

Due to the Floquet theorem, the double-time Fourier transformed retarded GF must take the form $\mathbf{G}^{r}(E,E') = \mathbf{G}^{r}(E,E+N\omega) = \mathbf{G}^{r}_{N}(E)$. The coupling of energies E and $E+N\omega$, where N is an integer, signifies how multiphoton processes assist the generation of pumped current. Since the heterostructures considered in Fig. 1 are translationally invariant in the transverse directions, we additionally perform a spatial Fourier transform, so that the multiphoton retarded GF depends on $\mathbf{k}_{\parallel} = (k_y,k_z)$ or $\mathbf{k}_{\parallel} = k_y$ in the case of heterostructures in Fig. 1(b) and Fig. 1(a), respectively.

In the absence of inelastic processes, solving $[E\check{\mathbf{1}} + \check{\mathbf{\Omega}} - \check{\mathbf{H}}_{\mathbf{k}_{\parallel}} - \check{\mathbf{\Sigma}}^{r}_{\mathbf{k}_{\parallel}}(E+\check{\mathbf{\Omega}})]\check{\mathbf{G}}^{r}_{\mathbf{k}_{\parallel}}(E) = \check{\mathbf{1}}$ for the multiphoton retarded GF is sufficient to obtain the time-averaged pumped spin current in N lead $p = L,R$ as [18]

$$I^{S_\alpha}_{p} = \frac{e}{2N_{\rm ph}}\int d\mathbf{k}_{\parallel}\,{\rm Tr}\,\{\hat{\sigma}_{\alpha}\check{\mathbf{\Gamma}}_{p,\mathbf{k}_{\parallel}}[\check{\mathbf{\Omega}},\check{\mathbf{G}}^{r}_{\mathbf{k}_{\parallel}}(E_F)\check{\mathbf{\Gamma}}_{\mathbf{k}_{\parallel}}(E_F)]\}, \tag{4}$$

where

$$[\check{\mathbf{\Omega}},\check{\mathbf{G}}^{r}_{\mathbf{k}_{\parallel}}(E_F)\check{\mathbf{\Gamma}}_{\mathbf{k}_{\parallel}}(E_F)] = \check{\mathbf{\Omega}}\check{\mathbf{G}}^{r}_{\mathbf{k}_{\parallel}}(E_F)\check{\mathbf{\Gamma}}_{\mathbf{k}_{\parallel}}(E_F) - \check{\mathbf{G}}^{r}_{\mathbf{k}_{\parallel}}(E_F)\check{\mathbf{\Gamma}}_{\mathbf{k}_{\parallel}}(E_F)\check{\mathbf{\Omega}}. \tag{5}$$

Here the adiabatic limit $\omega \ll E_F$ satisfied by the frequency of microwaves is taken into account, so that Eq. (4) is the Fermi surface property. By replacing the Pauli matrix $\hat{\sigma}_{\alpha}$ in Eq. (4) with the unit 2×2 matrix, we obtain the pumped charge current I_p. The symbol $\check{\mathbf{A}}$ denotes matrices which act in the total Hilbert space $\mathcal{H}_{\rm el}\otimes\mathcal{H}_{\rm ph}$, where the dimension of the Hilbert space of photons $\mathcal{H}_{\rm ph}$ is infinite and the dimension of $\mathcal{H}_{\rm el}$ is equal to the number of atomic orbitals comprising the central region. The unit matrix in the Hilbert space of a single electron $\mathcal{H}_{\rm el}$ is $\mathbf{1}$, and the unit matrix in $\mathcal{H}_{\rm el}\otimes\mathcal{H}_{\rm ph}$ is denoted by $\check{\mathbf{1}}$. In Eq. (4), $\check{\mathbf{\Omega}} = {\rm diag}\,(\ldots,-2\omega\mathbf{1},-\omega\mathbf{1},0,\omega\mathbf{1},-2\omega\mathbf{1},\ldots)$ is a diagonal matrix, and $\check{\mathbf{\Gamma}}_{\mathbf{k}_{\parallel}} = \sum_p \check{\mathbf{\Gamma}}_{p,\mathbf{k}_{\parallel}}$ is the level broadening matrix due to the coupling of the central region in Fig. 1 to N leads. Because the trace in the integrand, ${\rm Tr} \equiv {\rm Tr}_{\rm el}{\rm Tr}_{\rm ph}$, is summing over contributions from different photon exchange processes, the denominator includes $2N_{\rm ph}$ to avoid double counting. Importantly, the part of the trace operating in $\mathcal{H}_{\rm ph}$ space ensures the charge current conservation [18] *at each number* of exchanged microwave photons $N_{\rm ph}$ considered [note that often used solutions [36] to $\mathbf{G}^{r}_{N}(E)$ based on continued fractions generate artifactual charge current nonconservation, $\sum_p I_p \neq 0$, unless $N_{\rm ph}\to\infty$ is considered or the amplitude of the external potential is sufficiently small to make higher-order fractions negligible]. We find that considering $N_{\rm ph} = 10$ exchanged microwave photons is sufficient to obtain converged values for pumped spin and charge currents in heterostructures in Fig. 1.

In conclusion, inspired by the recent experiments [14,15] observing the conversion of pure spin current pumped by microwave-driven precessing magnetization into charge current flowing within the F/2DEG or F/TI interface—where conversion is due to strong interfacial SOC and it is unrelated to widely used [5–7] inverse SHE for conversion of pure spin currents into charge currents—we provide a unified theoretical treatment of this process together with spin-to-charge conversion when pumped spins flow perpendicularly through SO-coupled interfaces. Our approach is based on the charge-conserving Floquet-NEGF formalism [18,19] for open quantum systems driven by an external time-periodic potential, which makes it possible to quantify conversion efficiency I/I^{S_α} by computing *both* the charge and spin currents outflowing from such systems into the macroscopic reservoirs (such information has eluded recent alternative explanation of the experiments in Refs. [14,15] based on the nonequilibrium spin density-driven IEE [15,20]). The highest conversion efficiency $I/I^{S_\alpha} \simeq 40$–60% (depending on the precession cone angle) occurs when spins are pumped into the F/TI interface because of perfect spin-momentum locking on the surface of 3D TIs. On the other hand, even though conversion efficiency is orders of magnitude smaller for pumping vertically through the F/TI interface, we predict that converted charge current could be used as a sensitive probe for the presence of massive Dirac fermions at this interface which does not require a perfectly insulating bulk of TI or Fermi energy tuned into the energy gap induced by the magnetic proximity effect. We believe that these effects could also be used to quantify the magnitude of interfacial SOC in F/heavy-metal bilayers which provides one mechanism for recently emerged SO torques [37].

We thank L. Vila for insightful discussions. F.M. and B.K.N. were supported by NSF under Grant No. ECCS 1202069. N.N. was supported by Grant-in-Aids for Scientific Research (No. 24224009) from the Ministry of Education, Culture, Sports, Science and Technology of Japan, Strategic International Cooperative Program (Joint Research Type) from Japan Science and Technology Agency, and also by Funding Program for World-Leading Innovative R&D on Science and Technology (FIRST Program).

[1] J. Sinova and I. Žutić, Nat. Mater. **11**, 368 (2012).
[2] J. E. Hirsch, Phys. Rev. Lett. **83**, 1834 (1999).
[3] E. M. Hankiewicz, L. W. Molenkamp, T. Jungwirth, and J. Sinova, Phys. Rev. B **70**, 241301 (2004).
[4] C.-L. Chen, C.-R. Chang, and B. K. Nikolić, Phys. Rev. B **85**, 155414 (2012).
[5] E. Saitoh, M. Ueda, H. Miyajima, and G. Tatara, Appl. Phys. Lett. **88**, 182509 (2006).
[6] O. Mosendz, J. E. Pearson, F. Y. Fradin, G. E. W. Bauer, S. D. Bader, and A. Hoffmann, Phys. Rev. Lett. **104**, 046601 (2010).
[7] K. Ando, S. Takahashi, J. Ieda, Y. Kajiwara, H. Nakayama, T. Yoshino, K. Harii, Y. Fujikawa, M. Matsuo, S. Maekawa, and E. Saitoh, J. Appl. Phys. **109**, 103913 (2011).
[8] S. O. Valenzuela and M. Tinkham, Nature (London) **442**, 176 (2006).
[9] T. Seki, Y. Hasegawa, S. Mitani, S. Takahashi, H. Imamura, S. Maekawa, J. Nitta, and K. Takanashi, Nat. Mater. **7**, 125 (2008).
[10] C. Brüne, A. Roth, E. G. Novik, M. König, H. Buhmann, E. M. Hankiewicz, W. Hanke, J. Sinova, and L. W. Molenkamp, Nat. Phys. **6**, 448 (2010).
[11] D. A. Abanin, S. V. Morozov, L. A. Ponomarenko, R. V. Gorbachev, A. S. Mayorov, M. I. Katsnelson, K. Watanabe, T. Taniguchi, K. S. Novoselov, L. S. Levitov, and A. K. Geim, Science **332**, 328 (2011).
[12] Y. Kajiwara, K. Harii, S. Takahashi, J. Ohe, K. Uchida, M. Mizuguchi, H. Umezawa, H. Kawai, K. Ando, K. Takanashi, S. Maekawa, and E. Saitoh, Nature (London) **464**, 262 (2010).
[13] L. K. Werake, B. A. Ruzicka, and H. Zhao, Phys. Rev. Lett. **106**, 107205 (2011).
[14] J. C. R. Sánchez, L. Vila, G. Desfonds, S. Gambarelli, J. P. Attané, J. M. De Teresa, C. Magén, and A. Fert, Nat. Commun. **4**, 2944 (2013).
[15] Y. Shiomi, K. Nomura, Y. Kajiwara, K. Eto, M. Novak, K. Segawa, Y. Ando, and E. Saitoh, arXiv:1312.7091.
[16] R. Winkler, *Spin-Orbit Coupling Effects in Two-Dimensional Electron and Hole Systems* (Springer, Berlin, 2003).
[17] M. Z. Hasan and C. L. Kane, Rev. Mod. Phys. **82**, 3045 (2010); X.-L. Qi and S.-C. Zhang, *ibid.* **83**, 1057 (2011).
[18] F. Mahfouzi, J. Fabian, N. Nagaosa, and B. K. Nikolić, Phys. Rev. B **85**, 054406 (2012).
[19] S.-H. Chen, C.-L. Chen, C.-R. Chang, and F. Mahfouzi, Phys. Rev. B **87**, 045402 (2013).
[20] K. Shen, G. Vignale, and R. Raimondi, Phys. Rev. Lett. **112**, 096601 (2014).
[21] A. Takeuchi, K. Hosono, and G. Tatara, Phys. Rev. B **81**, 144405 (2010).
[22] J.-I. Ohe, A. Takeuchi, G. Tatara, and B. Kramer, Physica E **40**, 1554 (2008).
[23] Y. Tserkovnyak, A. Brataas, G. E. W. Bauer, and B. I. Halperin, Rev. Mod. Phys. **77**, 1375 (2005).
[24] S.-H. Chen, C.-R. Chang, J. Q. Xiao, and B. K. Nikolić, Phys. Rev. B **79**, 054424 (2009).
[25] W. Luo and X.-L. Qi, Phys. Rev. B **87**, 085431 (2013).
[26] Q. I. Yang, M. Dolev, L. Zhang, J. Zhao, A. D. Fried, E. Schemm, M. Liu, A. Palevski, A. F. Marshall, S. H. Risbud, and A. Kapitulnik, Phys. Rev. B **88**, 081407 (2013); P. Wei, F. Katmis, B. A. Assaf, H. Steinberg, P. Jarillo-Herrero, D. Heiman, and J. S. Moodera, Phys. Rev. Lett. **110**, 186807 (2013); A. Kandala, A. Richardella, D. W. Rench, D. M. Zhang, T. C. Flanagan, and N. Samarth, Appl. Phys. Lett. **103**, 202409 (2013).
[27] H. T. Ueda, A. Takeuchi, G. Tatara, and T. Yokoyama, Phys. Rev. B **85**, 115110 (2012).
[28] P. G. Silvestrov, P. W. Brouwer, and E. G. Mishchenko, Phys. Rev. B **86**, 075302 (2012); F. Zhang, C. L. Kane, and E. J. Mele, *ibid.* **86**, 081303 (2012).
[29] P.-H. Chang, F. Mahfouzi, N. Nagaosa, and B. K. Nikolić, Phys. Rev. B **89**, 195418 (2014).
[30] C.-X. Liu, X.-L. Qi, H. J. Zhang, X. Dai, Z. Fang, and S.-C. Zhang, Phys. Rev. B **82**, 045122 (2010).
[31] F. Mahfouzi and B. K. Nikolić, SPIN **3**, 1330002 (2013).
[32] E. Zhao, C. Zhang, and M. Lababidi, Phys. Rev. B **82**, 205331 (2010).
[33] G. Stefanucci and R. van Leeuwen, *Nonequilibrium Many-Body Theory of Quantum Systems: A Modern Introduction* (Cambridge University Press, Cambridge, 2013).
[34] P. W. Brouwer, Phys. Rev. B **58**, R10135 (1998).
[35] K. M. D. Hals, A. Brataas, and Y. Tserkovnyak, Europhys. Lett. **90**, 47002 (2010).
[36] B. Wang, J. Wang, and H. Guo, Phys. Rev. B **68**, 155326 (2003); K. Hattori, J. Phys. Soc. Jpn. **77**, 034707 (2008); T. Kitagawa, T. Oka, A. Brataas, L. Fu, and E. Demler, Phys. Rev. B **84**, 235108 (2011).
[37] K. Garello, I. M. Miron, C. O. Avci, F. Freimuth, Y. Mokrousov, S. Blügel, S. Auffret, O. Boulle, G. Gaudin, and P. Gambardella, Nat. Nanotech. **8**, 587 (2013); X. Fan, H. Celik, J. Wu, C. Ni, K.-J. Lee, V. O. Lorenz, and J. Q. Xiao, Nat. Commun. **5**, 3042 (2014).